Estimating Force Fields of Living Cells - Comparison of Several Regularization Schemes Combined with Automatic Parameter Choice

Sebastian Houben, Norbert Kirchgeßner, and Rudolf Merkel[1]

Forschungszentrum Jülich, IBN-4, 52425 Jülich, Germany {`n.kirchgessner,`
`r.merkel`}`@fz-juelich.de`

Abstract. In this paper we evaluate several regularization schemes applied to the problem of force estimation, that is Traction Force Microscopy (TFM). This method is widely used to investigate cell adhesion and migration processes as well as cellular response to mechanical and chemical stimuli. To estimate force densities TFM requires the solution of an inverse problem, a deconvolution. Two main approaches have been established for this. The method introduced by Dembo [1] makes a finite element approach and inverts the emerging LES by means of regularization. Hence this method is very robust, but requires high computational effort. The other ansatz by Butler [2] works in Fourier space to solve the problem by direct inversion. It is therefore based on the assumption of smooth data with little noise. The combination of both, a regularization in Fourier space, has been proposed [3] but not analyzed in detail. We cover this analysis and present several methods for an objective and automatic choice of the required regularization parameters.

1   Introduction

Living cells in multicellular organisms, e.g. sponges, mice and men, are constantly experiencing and, most often, generating mechanical forces. These are essential in a plethora of physiological and pathological processes ranging from stem cell differentiation and tissue formation during embryogenesis to cell locomotion in the cellular immune response and cancer metastasis. Any attempt to quantitatively understand such processes crucially depends on spatially and temporally highly resolved measurements of cell forces. The first reliable technique to visualize forces of individual cells was pioneered by Harris et al. [4] who grew cells on a thin silicone sheet and observed wrinkles emerging under contracting cells. To estimate the acting traction forces the setup was slightly changed by replacing the silicone sheet with a solidly supported thin film of elastic material. Usually cross-linked polyacrylamide (PAA) [1] or polydimethylsiloxane (PDMS) [5], [6] are used. Fluorescent marker beads are embedded slightly below the surface. These markers can be localized by fluorescent light microscopy combined with digital image processing (c.f. Sect. 2). By comparison to a reference image where the cell has been removed mechanically and the rubber has reached its relaxed state the cell force induced deformations can be quantified (see Fig. 1).
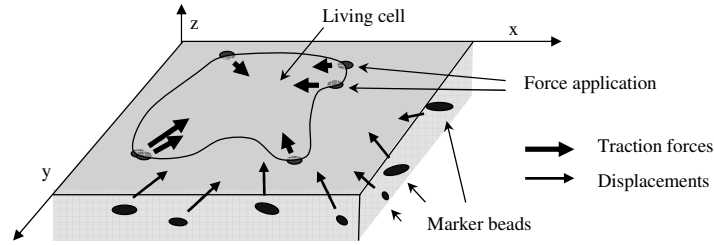
Fig. 1: Scheme of the experimental setup for traction force analysis. A cell is located on a thin rubber film with embedded marker beads and exerts forces on it. The position of the fluorescent beads can be detected with fluorescence microscopy and quantified by digital image processing (c.f. Sect. 2). The deformation vector field is subsequently used to estimate location and magnitude of the cell force (see Sect. 3). Please note that the proportions are not realistic.

To find a mathematical model that relates the measured deformations to the traction forces the silicone substrate layer is most often assumed to be infinitely thick, i.e., a linear elastic halfspace. Furthermore, the tractions are restricted to act only on the surface of the halfspace. This kind of problem was studied in elasticity theory by Boussinesq [7], [8] and found to satisfy the following Fredholm integral equation

$$\int_{\mathbb{R}^2 \backslash \{y\}} G(y - x)f(x)dx = u(y) \text{ for each } y \in \mathbb{R}^2 \text{ or short } \mathcal{G}[f] = u \ , \quad (1)$$

where $u : \mathbb{R}^2 \mapsto \mathbb{R}^2$ denotes the deformation at a place y, $f : \mathbb{R}^2 \mapsto \mathbb{R}^2$ the force at a location x and G the Boussinesq Greens' Tensor

$$G(d) = \frac{3}{4\pi E |d|^3} \begin{pmatrix} |d|^2 + d_1^2 & d_1 d_2 \\ d_1 d_2 & |d|^2 + d_2^2 \end{pmatrix} \text{ with } d = (d_1, d_2)^T \in \mathbb{R}^2 \ . \quad (2)$$

For notational clarity we use the uncommon $\mathcal{G}[f]$ for the linear operator $\mathcal{G}$ acting on f. E is the rubber's Young modulus. Its Poisson ratio was found to be 0.5 [6] corresponding to an incompressible medium. Merkel et al [9] have shown that the assumption of an infinite halfspace has to be dropped if the layer thickness is less than 60 μm. Here a modified Greens' Tensor must be used, c.f. [9].

For both the finite and the infinite thickness case we must therefore invert a Fredholm integral equation, a procedure which is known to be ill-posed. It hence requires a regularization ansatz. We briefly introduce the methods of Dembo and Butler in Sects. 1.1 and 1.2, several possibilities combining both methods are discussed in Sect. 3.

1.1   Finite Element Method

To discretize the integral equation (1) Dembo used the manually marked cell outline and generated a quadrilateral mesh within for estimating traction den-

sities. Cell forces are therefore restricted to the cell area. This is a reasonable assumption and limits the complexity of the emerging equation system. However, after discretization the LES is still ill-posed and normally even lacks a solution. To circumvent this Dembo made use of the regularization functional

$$||\mathcal{G}[f] - u||^2 + \lambda \Omega(f) \tag{3}$$

whose minimum is a force distribution f that compromises between the measured data set u and the operator Ω. In Dembo's method an entropy measure is used to prefer smooth force fields. The regularization parameter $\lambda \geq 0$ is used to adjust the expected complexity of the solution. Dembo's method is known to be highly accurate and profits from the restriction to the force application area, which stabilizes the algorithm and restrains the number of unknowns. Nevertheless, f is still high-dimensional and the minimization of the functional (3) is computationally expensive.

1.2   Fourier Method

Since the left-hand side of Equation (1) is a convolution, a transformation to Fourier space will reduce it to a simple product

$$\hat{G}(k)\hat{f}(k) = \hat{u}(k) \text{ for each } k \in \mathbb{R}^2 \ , \tag{4}$$

where $\hat{G}, \hat{f}, \hat{u}$ respectively denote the Fourier transforms of G, f, u and k is a two dimensional wave number. Note that for each k Equation (4) is a LES with two equations and two unknowns while the Dembo's LES is a system with $2n$ equations and $2m$ unknowns. Here the number of beads is denoted by n and m is the number of forces. The inversion of (4) is therefore very fast. However, for small k the matrix $\hat{G}$ is nearly singular and a good solution will hence crucially depend on noise-free data as mentioned by Butler et al [2].

2   Digital Image Processing

Several methods are currently in use to track fluorescent marker beads in micrographs. All of them are comparably fast, accurate and reliable. In our case we used a tracking algorithm that was implemented and described earlier [9]. Briefly, the method comprises two steps. First, an interactively marked sample bead of the reference image is fitted by a two dimensional Gaussian to obtain a template. This is then compared to the whole image by normalized cross-correlation. Local maxima of the thresholded correlation function are assumed to be probable bead positions. Second, from each of these initial positions in the reference image a template is taken and cross-correlated to a certain vicinity in the image of the strained rubber. Templates that are recognized above a preselected threshold are taken into account for the deformation vector field.

3   Regularization

In the following we suggest a combination of both Dembo's and Butler's method, a regularization in Fourier space, aiming to connect the stabilizing effects of the regularization approach with the fast computation of a fourier space scheme. Such a combined method has already been proposed by Sabass et al [3] albeit without quantitative analysis of the possible regularization schemes and with a manual choice of the regularization parameter. For this purpose we interpolate the scattered deformation vector field on a rectangular grid. Let g_x, g_y be the grid numbers and x_{min}, x_{max}, y_{min} and y_{max} minimum and maximum x- and y-coordinate of the n bead positions, respectively. By choosing

$$g_x := \left\lfloor \sqrt{n \frac{y_{max} - y_{min}}{x_{max} - x_{min}}} \right\rfloor \text{ and } g_y := \left\lfloor \frac{n}{g_x} \right\rfloor \tag{5}$$

we guarantee that the number of displacement vectors and the aspect ratio of the definition area stay approximately the same. Please note that by this choice the spatial resolution of our TFM method is already determined ($\lfloor x \rfloor :=$ $\max_{k \in Z, k \leq x}(k)$). In a next step we perform a FFT on the interpolated deformation field to obtain $\tilde{u}$ and[1] likewise wave numbers $k_{1,x}, k_{1,y}..., k_{n,x}, k_{n,y} \in \mathbb{R}$. We now approach equation (4) for these k. For convenience, let

$$\tilde{G} := \begin{pmatrix} \hat{G}(k_{1,x}) & & \\ & \ddots & \\ & & \hat{G}(k_{n,y}) \end{pmatrix} . \tag{6}$$

We retrieve the LES

$$\tilde{G}\tilde{f} = \tilde{u} \ . \tag{7}$$

A back transformation of its solution[2] $\tilde{f}$ gives a force density on the grid that $\tilde{u}$ was interpolated on. However, the blocks of $\tilde{G}$ are nearly singular for small values of k and must hence be regularized. For reasons of computational efficiency and convenient implementation we restrict ourselves to a slightly generalized version of the regularization procedure by Tikhonov [10]. In fact we make use of the following functional:

$$||\tilde{G}\tilde{f} - \tilde{u}||^2 + \lambda||L(\tilde{f} - f_0)||^2 \ , \tag{8}$$

where L is a quadratic matrix and f_0 is a vector of the same dimension as $\tilde{f}$. The minimum of this functional is known to be the solution of

$$(\tilde{G}^*\tilde{G} + \lambda L^*L)\tilde{f} = \tilde{G}^*\tilde{u} + \lambda L^*Lf_0 \tag{9}$$

that is guaranteed to be unique if L is injective. Minimization of (8) is therefore unexpensively accomplished by direct inversion of (9). Choosing L and f_0 is

---

[1] $\tilde{u}$ is a vector containing x- and y- coordinates of the Fourier-transformed deformation vectors in the grid which is assigned linewise.

[2] $\tilde{f}$ is unique because $\tilde{G}$ is blockwise non-singular

equivalent to selecting a suitable penalty term for equation (8). L is normally chosen to be a measure of a property that the solution is expected to have while f_0 can be understood to be an approximation of the solution itsself. There are procedures that allow the definition of an optimal L using a Bayesian approach with a prior of the solution's noise distribution. Because traction force patterns have never been measured by direct methods, the essential information for the Bayesian interpretation is unavailable. Instead we will evaluate several heuristic methods that are based on reasonable assumptions of location, formation and temporal evolution of the traction field.

3.1   Classic Approaches

A first attempt to stabilize (7) is to penalize high values of $\tilde{f}$ by setting $L = I$ as proposed by Tikhonov [10]. Since the equations that belong to small wave numbers are more instable than those to large ones, it also seems reasonable to penalize high Fourier coefficients for small wave numbers.[3] For this we made the following choices we call wave damp or wave damp square choosing

$$L_{ij} := \delta_{ij}\frac{1}{|k_i|} \qquad \text{or} \qquad L_{ij} := \delta_{ij}\frac{1}{|k_i|^2} \ . \tag{10}$$

3.2   Temporal Smoothing

In many cases a series of cell and substrate images is made to record the cell's activity. If we assume that the difference of forces from image to image is small we can develop another penalty term. Let $t_1, ..., t_l \in \mathbb{R}$ be the points of time the images were made and $u^{(t_i)}$ the respective deformation and forces at those points of time. If we set

$$\bar{G} := \overbrace{\begin{pmatrix} \tilde{G} & & \\ & \ddots & \\ & & \tilde{G} \end{pmatrix}}^{l \text{ times}} \qquad \text{and} \qquad \bar{u} := \begin{pmatrix} u^{(t_1)} \\ \vdots \\ u^{(t_l)} \end{pmatrix} \tag{11}$$

the solution of $\bar{G}\bar{f} = \bar{u}$ will give a force density estimation for the whole series of images. We can now introduce our assumptions of little difference by applying

$$L_{ij} := \delta_{ij} - \delta_{i(j-2n)} \ , \tag{12}$$

i.e. the penalty term sums the differences between the fourier coefficients in one time step and the proceeding. Thus, the functional (8) will prefer solutions where the forces at the different points of time only change slightly.

---

[3] With ground truth we could isolate the critical frequencies for an optimal L.

3.3   Restriction to a Predefined Area

An important advantage of Dembo's finite element method is that it easily allows the force to be estimated only within a predefined area. By transforming the convolution (1) into Fourier space this seems to become impossible since the FFT algorithm works on a rectangular grid. However, it is possible to effectively restrict forces to a certain area by the following procedure. Let $1_C : \mathbb{R}^2 \mapsto \{0, 1\}$ be the indicator function for the cell area, i.e., $1_C(x)$ yields 1 if and only if x is within the cell area.

The procedure consists of two steps. First we solve equation (7) by a common regularization scheme (c.f. Sects. 3.1 and 3.2) to get a solution $\tilde{f}$. We now transform $\tilde{f}$ into spatial domain and multiply the result with 1_C. The product will be 0 outside the predefined area and return the estimated force pattern inside. Subsequently we retransform the product into Fourier space and call the final result f_0. In a second step we make use of the functional

$$||G\tilde{f} - \tilde{u}||^2 + \lambda||\tilde{f} - f_0||^2 \tag{13}$$

to get a solution that implicitly prefers a resemblance to the function f_0, i. e., it has no significant forces outside the marked cell area.

3.4   Objective Choice of the Regularization Parameter

Crucial to all regularization methods is the choice of the parameter λ that is supposed to balance the data discrepancy and the penalty term. Therefore it is of high importance to use well founded values for λ.[4] To automate this parameter choice without knowledge of the error several procedures have been proposed of which two proved especially useful for our case.

The heuristic idea of the L-curve criterion [11] is to find a λ that represents a trade-off between data fidelity and the penalty norm. This balance can be determined by examining the L-shaped curve $(||Gf_\lambda - u||, ||L(f_\lambda - f_0)||)$ where f_λ is the solution of (9) but for our purpose this method proved unstable. Instead we determine the functions $d(\lambda) = ||Gf_\lambda - u||$ and $p(\lambda) = ||L(f_\lambda - f_0)||$ and identify the λ values at which d has maximum and p has minimum derivative. The average of those two values subsequently provides a useful choice for the regularization parameter since it determines the value where the penalty starts to apply and the data is still sufficiently fitted by the model.

Another parameter choice yielding a very good performance is an adjusted cross-validation approach [12]. The cv-method splits the data set into a validation and computation set. A ratio of 25% to 75% is a common choice. While the computation set is used to calculate a solution for several choices of λ, these solutions are applied to the direct problem and the result is compared to the

---

[4] With the Bayesian approach that was previously mapped out, λ turns out to be optimally chosen as ratio of the squared deformation error and the squared error in the force field.

validation set. The solution that suits best is the one that most likely can explain the unused data and is therefore a reasonable choice.

Since a cross-validation in Fourier space did not provide satisfying results we adapted it to work in position space. The computation set is interpolated on a grid, transformed into Fourier space and forces are estimated as described above. By equation (7) we are now able to compute the deformation vector field u_λ that would be observed if the estimation f_λ was accurate. u_λ is retransformed to position space and the difference d_λ to the grid-interpolated validation set is determined. The λ which minimizes d_λ is the parameter to choose. It is possible to repeat this procedure with another 25% validation set to stabilize the results. Thus, the cross-validation approach is very reliable but computationally expensive.

4   Experiments and Results

We evaluated our approach on several data to test it with ground truth and different levels of noise in displacement data. First we created a synthetic set of test data (see Fig 2, first row, left). The second situation was force fields of normal human epidermal keratinocytes (Young modul of substrate: 11 kPa) as retrieved by Tikhonov regularization and the L-curve criterion. (see Fig 2, first row, right). This enables us to test the traction estimation in a realistic situation. Both traction distributions served as ground truth for our second test on synthetic data with known ground truth and noise.

4.1   Simulations

Simulations were performed by adding normal distributed noise on ground truth displacements. For each noise level we performed the simulation with 20 different noise patterns. To avoid random fluctuations between the tested penalties and parameter determinations we used the same noise patterns for all simulations.

Noise levels were chosen as multiples of the occuring mean displacements in the test images. As the interpretation of this quantity is not obvious we show the displacement vector fields with the highest noise level in Fig. 2, second row. All tests were done with 7 different noise levels.

On all data we performed tests with the wave damp, squared wave damp, classical Tikhonov regularization and the temporal derivative as regularization penalties. For determination of the regularization parameter we used both, the L-curve criterion and the cross-validation approach with and without restricting the traction to the cell area.

4.2   Results

Results for the artificial test pattern are shown in Fig. 3. Wave damp and squared wave damp regularization generally show a linear dependence of estimation error on the noise level up to a certain point. The error without any regularization is
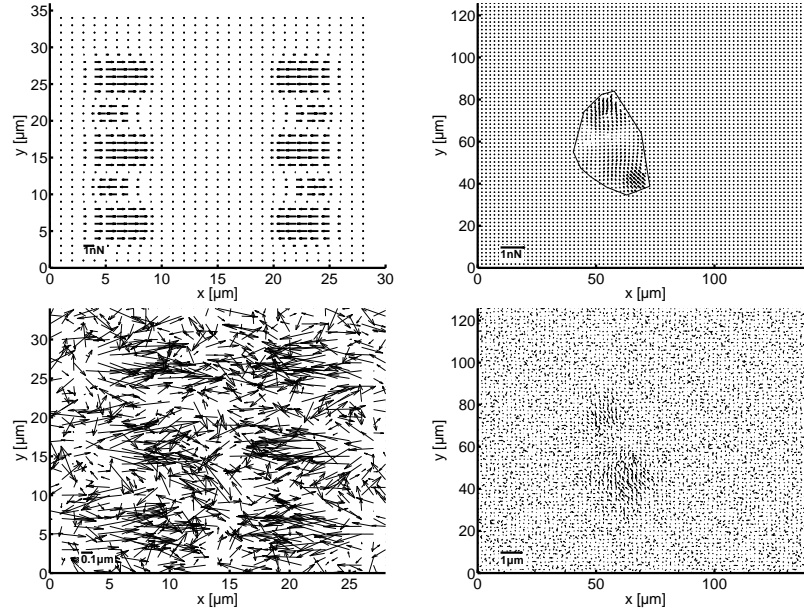
Fig. 2: Synthetic test data. First row: Defined traction patterns. Left: Artificial test pattern. Right: Estimated traction distribution of a normal human epidermal keratinocyte. Second row: Synthetic displacement data with maximum of added noise. Left: Displacements of artificial test pattern, standard deviation of noise: 0.14 μm. Right: Displacement of estimated traction distribution of a normal human epidermal keratinocyte, standard deviation of noise: 0.054 μm.

also shown. The temporal derivative of the traction is therefore not well suited for estimation in Fourier space. This was surprising since for the well-known point force traction estimation as mapped out in [3], we found it a stable improvement. Classical Tikhonov regularization combined with cross-validation yields best accuracy. This result is confirmed by the simulations with the realistic traction distribution (cf. Fig. 3, 3rd and 4th row). The squared wave damp regularization also provides good results for high noise levels.

For low noise the cross-validation is not suited for the choice of an appropriate regularization parameter which leads to high deviations (see Fig 3, 3rd row right, for noise lower than 2 times of the mean displacement $\lambda < 10^{-6}$, for higher noise levels $\lambda > 10^6$). The second step regularization restricting the forces to the cell area was able to enhance the results in several cases. Due to its low computational effort the second step should be considered whenever the force application area is known.

5   Discussion

In this paper we presented a systematic investigation of wave damp, wave damp squared, Tikhonov regularization and temporal derivative as penalties for trac-

tion estimation in Fourier space. The regularization parameter estimation was performed for all penalties with automatic choice of the regularization parameter λ inspired by the L-curve criterion and cross-validation each with and without constraining the tractions to the cell area. In connection with the Tikhonov regularization cross-validation yielded the best results. For this combination the estimation errors are less than a fifth of the straight forward, not regularized solution. As the choice of λ is critical for the evaluation of displacement data we see an important point in its automized choice. This enables an objective and reproducible evaluation of large data sets comprising many images.

6   Acknowledgements

References

1. Dembo, M., Oliver, T., Ishihara, A., Jacobson, K.: Imaging the traction stresses exerted by locomoting cells with the elastic substratum method. Biophysical Journal **70** (1996) 2008 – 2022
2. Butler, J.P., Tolic-Norrelykke, I.M., Fabry, B., Fredberg, J.J.: Traction fields, moments, and strain energy that cells exert on their surroundings. American journal of physiology, Cell physiology **282** (2002) C595 – 605 DOI:10.1152/ajpcell.00270.2001.
3. Sabass, B., Gardel, M.L., Waterman, C.M., Schwarz, U.S.: High resolution traction force microscopy based on experimental and computational advances. Biophysical Journal **94** (2008) 207 – 220 DOI:10.1529/biophysj.107.113670.
4. Harris, A.K., Wild, P., Stopak, D.: Silicone rubber substrata: a new wrinkle in the study of cell locomotion. Science **208** (1980) 177 – 179 DOI: 10.1126/science.6987736.
5. Balaban, N.Q., Schwarz, U.S., Riveline, D., Goichberg, P., Tzur, G., Sabanay, I., Mahalu, D., Safran, S., Bershadsky, A., Addadi, L., Geiger, B.: Force and focal adhesion assembly: a close relationship studied using elastic micropatterned substrates. Nature Cell Biology **3** (2001) 466 – 472
6. Cesa, C.M., Kirchgeßner, N., Mayer, D., Schwarz, U., Hoffmann, B., Merkel, R.: Micropatterned silicone elastomer substrates for high resolution analysis of cellular force patterns. Rev. Sci. Instrum. **78** (2007) 034301–1 – 034301–10
7. Boussinesq, J.: Applications des potentiels a l'etude de l'equilibre et du mouvement des solides elastiques. Gauthier-Villars, Paris (1885)
8. Landau, L.D., Lifshitz, E.M.: Lehrbuch der Theoretischen Physik: Elastizitaetstheorie. Volume 7. Akademie-Verlag, Berlin (1987) Deutsche Uebersetzung.
9. Merkel, R., Kirchgeßner, N., Cesa, C.M., Hoffmann, B.: Cell force microscopy on elastic layers of finite thickness. Biophysical Journal **93** (2007) 3314–3323
10. Tikhonov, A.N.: On the solution of ill-posed problems and the regularization method. Dokl. Akad. Nauk SSSR **151** (1963) 501 – 504
11. Hansen, P.C.: Analysis of discrete ill-posed problems by means of the L-curve. SIAM Review **34** (1992) 561 – 580
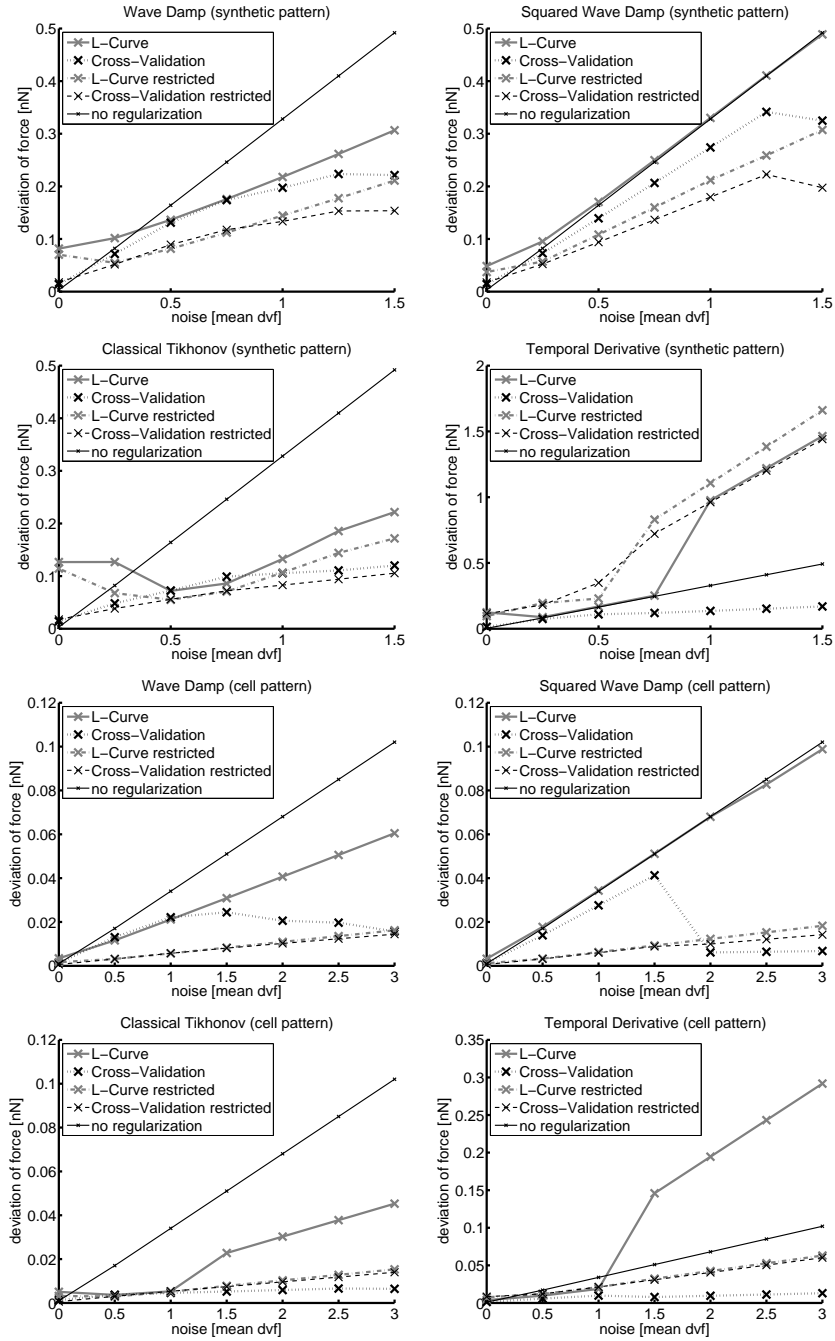12. Wahba, G.: Spline models for observational data. SIAM, US (1990)

Fig. 3: Results of different penalty terms on the evaluation of artificial test data (first two rows) and a realistic traction distribution (last two rows) using different estimation methods for the regularization parameter λ. First row left: wave damp, right: wave damp squared. Second row left: Tikhonov, right: temporal derivative with 5 time steps considered, note the different scaling. Third row left: wave damp, right: wave damp squared. Fourth row left: Tikhonov, right: temporal derivative with 5 time steps considered, note the different scaling.